Sophia Haussener[1]
Department of Mechanical Engineering,
EPFL,
1015 Lausanne, Switzerland
e-mail: Sophia.haussener@epfl.ch

Iwan Jerjen

Peter Wyss

Department of Electronics/Metrology,
EMPA Material Science and Technology,
Überlandstrasse 129,
8600 Dübendorf, Switzerland

Aldo Steinfeld
Department of Mechanical and Process Engineering,
ETH Zurich,
8092 Zurich, Switzerland;

Solar Technology Laboratory,
Paul Scherrer Institute,
5232 Villigen, Switzerland

Tomography-Based Determination of Effective Transport Properties for Reacting Porous Media

The effective heat and mass transport properties of a porous packed bed of particles undergoing a high-temperature solid–gas thermochemical transformation are determined. The exact 3D geometry of the reacting porous media is obtained by high-resolution computed tomography. Finite volume techniques are applied to solve the governing conservation equations at the pore-level scale and to determine the effective transport properties as a function of the reaction extent, namely, the convective heat transfer coefficient, permeability, Dupuit–Forchheimer coefficient, tortuosity, and residence time distributions. These exhibit strong dependence on the bed morphological properties (e.g., porosity, specific surface area, particle size) and, consequently, vary with time as the reaction progresses. [DOI: 10.1115/1.4004842]

Keywords: packed bed, solar energy, gasification, chemical reactors, effective properties, tomography, heat transfer, mass transfer

1 Introduction

Packed-bed reactors containing porous media are commonly used in solid–gas thermochemical processing because of their high contacting area. Of interest are packed-bed reactors for producing solar fuels, which make use of concentrated solar radiation as the energy source of process heat [1]. Examples of these high-temperature solar-driven processes are the thermal reduction of ZnO as part of a H_2O-splitting cycle and the thermal gasification of carbonaceous material for producing syngas [2,3]. The design, optimization, and scale-up of packed-bed reactors require modeling the transport phenomena across porous media. Volume averaging models [4] are commonly applied to reduce complexity and computational time. Their accuracy relies heavily on the accurate determination of the effective heat/mass transport properties of the reacting porous media, such as the convective heat transfer coefficient and permeability. The bed morphology and its effective heat/mass transport properties can vary significantly as the reaction progresses, but these variations are often neglected, introducing additional inaccuracies in the continuum models.

Empirical Nusselt correlations for nonreacting packed beds have been derived for solid–fluid heat transfer in packed beds based on a combination of Nu for laminar and turbulent flows around a single sphere [5], on an experimental fit that accounts for axial dispersion [6], on a stochastic model of the packed bed geometry [7], and on an experimental fit to a numerical continuum model [8]. Heuristic and empirical models for permeability and Dupuit–Forchheimer coefficient in porous media include approximation of the porous structure as parallel channels [9,10] and as parallel or perpendicular cylinders or spheres [11–13], permeability bound model based on the mean survival time [14], and high Reynolds flow models [15,16]. A promising experimental-numerical technique has been developed to calculate the heat transfer coefficient of reticulate porous ceramic foams, which involves direct pore-level simulation (DPLS, also called explicit numerical simulation) applied on the exact foam geometry determined by computed tomography [17,18]. This technique can also be applied to determine heat transfer coefficients, permeability and Dupuit–Forchheimer coefficients for reacting packed beds. In this study, we apply DPLS on the exact geometry determined by computed tomography (CT). Either lattice-Boltzmann method and lattice-gas automata [19–22] or finite differences and finite volume (FV) techniques [17–19,21,23] are used to solve the governing Navier–Stokes equations for the velocity and pressure fields. Recently, CT-based DPLS of a packed bed undergoing a solid–gas thermochemical transformation was applied to characterize its morphological and radiative transport properties as a function of the reaction extent [24]. This paper deals with the determination of the reaction extent-dependent heat transfer coefficient, permeability, Dupuit–Forchheimer coefficient, tortuosity, and residence time distributions of a reacting packed bed. The exact 3D geometry of the packed bed containing complex, porous, and nonspherical particles is determined as a function of the reaction extent by high-resolution CT.

The effective transport properties obtained in this study account for the morphological changes during the reaction and thus enable for more detailed and accurate continuum models. Specifically, the methodology is applied for the solar-driven gasification of carbonaceous materials in a packed-bed reactor configuration.

2 Sample Preparation and Characterization

The model reaction selected is the solar-driven thermochemical conversion—by combined pyrolysis and gasification—of carbonaceous materials to high-quality syngas [3]. Syngas, a mixture of mainly H_2 and CO, can be used to fuel efficient combined cycles or fuel cells for power generation, or further processed to hydrogen or liquid fuels for transportation. Pyrolysis, which involves the thermal decomposition and devolatilization of the feedstock, takes place prior to the gasification, which involves the heterogeneous solid–gas reaction of char with reactive gases (e.g., H_2O or CO_2). The combined pyrolysis and gasification of the carbonaceous

[1]Corresponding author.

Contributed by the Heat Transfer Division of ASME for publication in the Journal of Heat Transfer. Manuscript received April 16, 2011; final manuscript received July 30, 2011; published online October 27, 2011. Assoc. Editor: Walter W. Yuen.

Table 1 X_C, $d_{med,ex}$, ε_{ex}, and ε_{num} for the three samples of packed bed investigated

	X_C	$d_{med,ex}$ (mm)	ε_{ex}	ε_{num}
Initial	0	1.14	0.60 ± 0.05	0.61
Char	0.68	0.97	0.86 ± 0.05	0.74
Ash	1	0.42	0.82 ± 0.28	0.65

feedstock is carried out in a laboratory packed-bed reactor to produce samples of the reacting solid material at different reaction extents under controlled reaction conditions. The experimental setup has been described previously in detail [24]. The experimental procedure consists of pyrolysis at 1000 K (heating rate approx. 90 K/min) in an inert atmosphere followed by gasification at 1273 K in a steam partial pressure of 0.8 bar. The selected carbonaceous material is waste tire shreds because of their promising recycling application. Samples of the packed bed are obtained for a reaction extent $X_C = 0$ (initial), after pyrolysis at $X_C = 0.68$ (char), and after gasification at $X_C = 1$ (ash). X_C is determined by the carbon conversion based on mass balance. The samples at predefined X_C were obtained by stopping the reaction (shutting down heating and reacting gas inflow) and subsequent cooling (rate approx. 70 K/min) the packed bed in an oxygen free atmosphere. The variation of the porosity due to changes in the operational conditions (temperature, pressure, etc.) was of the same order of magnitude as the standard deviation of the experimental results [24].

Elemental analysis of the tire shreds indicates 82 wt. % C, 7 wt. % H, 3 wt. % O, 2 wt. % S, and heavy metal impurities. Fixed carbon represents 29 wt. %. Median particle diameter, $d_{med,ex}$, experimentally determined by laser scattering (HORIBA LA-950 analyzer) and porosity, ε_{ex}, experimentally determined by weight measurements, are listed in Table 1 for the three X_C of the packed bed. Additionally listed is the numerically calculated porosity, ε_{num}, defined as

$$\varepsilon_{num} = \frac{N_{vox,void}}{N_{vox,tot}} \tag{1}$$

and calculated based on the CT data (see Sec. 3). The initial increase in porosity is due to the release of volatiles during pyrolysis, resulting in highly porous, fractured, and nonspherical particles. During char gasification, the particles shrink and break apart, reducing overall bed porosity.

3 Computed Tomography

High-resolution CT is carried out on the tomographic microscopy and coherent radiology experiments (TOMCAT) beamline at the Swiss Light Source (SLS) of the Paul Scherrer Institute [25,26] for 23 keV photon energy, 400 μA beam current, 940 ms exposure times, and 1500 projections. The resulting tomographic data have voxel size of 3.7 μm and investigated field of view (FOV) of $7.6 \times 7.6 \times 3.5$ mm^3. Exemplary tomograms of the packed beds are shown in Fig. 1. Due to large image distortion of the ash sample, tomographic data for the ash sample are obtained with a microfocal x-ray tube source, resulting in a voxel size of 5 μm and a FOV of $5.6 \times 5.6 \times 6$ mm^3. Phase segmentation is achieved by a local mode method. Adjustment of ε_{ex} and ε_{num} is not used for threshold selection since it results in wrong phase segmentation due to insufficient resolution of the nanopores, which account for 10–20% of the porosity.

4 Methodology

DPLS is applied on the packed-bed geometry obtained by high-resolution CT, following the methodology previously developed for reticulate porous ceramic foams [17,18]. A schematic of the DPLS domain is shown in Fig. 2 and consists of a square duct containing a sample of the packed bed and an undisturbed inlet and outlet region. The coupled continuity, momentum, and energy conservation equations in the (laminar) fluid phase are solved by FV techniques at the pore-level scale [27]. Temperature, T_0 (=300 K), and velocity, u_0, are given at the inlet. Temperature, T_{sf} (=1273 K), and no-slip condition are given at the solid–fluid boundary. The lateral walls of the duct, including the sample, are assumed symmetric. Pressure, p_{atm} (= 1 atm), is given at the outlet. The boundary conditions are

$$\bar{\mathbf{u}} = 0, T = T_{sf} \text{ at the solid-fluid interface} \tag{2}$$

$$\bar{\mathbf{u}} \cdot \hat{\mathbf{n}} = 0, \hat{\mathbf{n}} \cdot \nabla \bar{\mathbf{u}} = 0, \mathbf{q}'' \cdot \hat{\mathbf{n}} = 0 \text{ at the lateral walls} \tag{3}$$

$$\bar{\mathbf{u}} \cdot \hat{\mathbf{n}} = -u_0, \; T = T_0 \text{ at the inlet} \tag{4}$$

$$p = p_{atm} \text{ at the outlet} \tag{5}$$

The velocity, pressure, and temperature distributions are computed within the fluid phase and the heat fluxes are computed through the solid–fluid boundary. A sample with dimensions of $4.7 \times 4.7 \times 2.3$ mm^3 is used for the calculations, limited by the FOV of the CT scans. This volume satisfies the definition of a representative elementary volume (REV, smallest volume for which continuum is still valid) as porosity calculated in growing cubic subvolumes converge within a band of ± 0.054 (γ) for cubic volumes with edge length of 3.7 mm ($l_{REV,\gamma=0.054}$):

$$l_{REV,\gamma} = \min\left\{ l \le \tilde{l} \middle| \varepsilon_{num} - \gamma < \varepsilon\left(\tilde{l}^3\right) < \varepsilon_{num} + \gamma \right\} \tag{6}$$

Additionally, the mean free path of the gases involved are below 0.532 μm (H_2 at 1 atm and 1273 K), which is 14 times smaller than the CT resolution and consequently the smallest pores detectable. Therefore, continuum for the fluid phase is assumed.

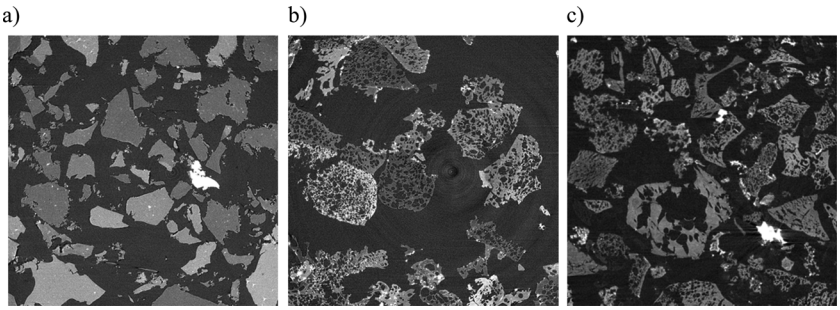

Fig. 1 CT scans of samples of the packed bed of tire shreds at three reaction extents: (*a*) initially at $X_C = 0$; (*b*) after pyrolysis at $X_C = 0.68$ (char); and (*c*) after gasification at $X_C = 1$ (ash). The edge length is 5.2 mm.

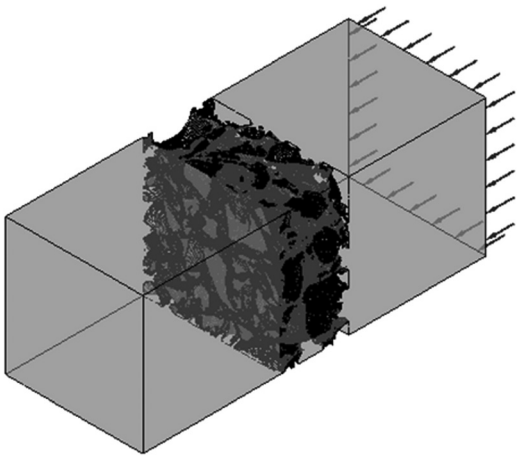

Fig. 2 Schematic of the DPLS domain, consisting of a square duct containing a sample of the packed bed, and inlet and outlet regions

Convergence of the numerical calculation is achieved for a terminal residual RMS of the iterative solution below 10^{-4} and for a maximal mesh element length of 90 μm (initial and char) and 117 μm (ash). The meshes are composed of approximately 3.5×10^7 tetrahedral elements. The meshed domain of the initial packed bed is shown in Fig. 3. The mesh is generated by an in-house mesh generator for unstructured body-fitted grids [17,18]. Two quad-core Intel Xeon 2.5 GHz processors and 32 GB random access memory (RAM) are used to solve the governing equations in approximately 24 h. Alternatively, using 12 Advanced Micro Devices, Inc. (AMD) Opteron 2.5 GHz processors and 42 GB RAM of ETH's high-performance cluster Brutus reduces computational time by 1/3.

5 Heat Transfer—Convection

5.1 Theory and Results. The convective heat transfer coefficient between the solid and the fluid phase is calculated by

$$h_{sf} = \frac{\int_{A_{sf}} q'' dA_{sf}}{A_{sf} \cdot \Delta T_{lm}} \tag{7}$$

and fitted to a correlation of the form

$$\mathrm{Nu} = a + b\mathrm{Re}^c \mathrm{Pr}^d \tag{8}$$

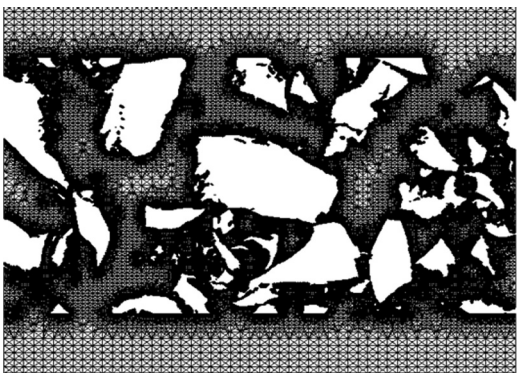

Fig. 3 Mesh cutting plane of the computational domain of the initial packed bed. The packed bed region is enlarged. Parts of the inlet and outlet regions are visible at the top and bottom.

Table 2 Numerically determined and fitted Nu correlations for the three different reaction extents of the packed bed

	Nu	RMS
Initial ($X_C = 0$)	$8.399 + 0.234\mathrm{Re}^{0.909}\mathrm{Pr}^{0.627}$	3.928
Char ($X_C = 0.68$)	$0.754 + 0.091\mathrm{Re}^{0.740}\mathrm{Pr}^{0.570}$	0.288
Ash ($X_C = 1$)	$4.592 + 0.274\mathrm{Re}^{0.886}\mathrm{Pr}^{0.684}$	2.338

The numerically calculated and fitted Nu correlations for the packed bed at different X_C are given in Table 2. Figure 4 shows the numerically calculated Nu numbers for the packed bed at $\mathrm{Pr} = 0.1$, 1, and 10 and their fits.

Nu decreased during pyrolysis and increased during gasification as a result of morphological changes during the reaction. During pyrolysis, the formation of direct flow paths across the packed bed reduced the accessible surface area for convective heat exchange between the two phases. During gasification, the break-up of particles increased the accessible surface area for heat exchange.

The four constants of the Nu correlation, Eq. (8), are related to the reaction extent by a 2nd-order polynomial function, assuming that the morphological parameters influencing the Nu correlation (e.g., ε and A_0) can be related to X_C by a 2nd-order polynomial function

$$a(X_C) = 23.92X_C^2 - 27.66X_C + 8.34 \tag{9}$$

$$b(X_C) = 0.83X_C^2 - 0.79X_C + 0.23 \tag{10}$$

$$c(X_C) = 0.74X_C^2 - 0.76X_C + 0.91 \tag{11}$$

$$d(X_C) = 0.47X_C^2 - 0.42X_C + 0.63 \tag{12}$$

Thus, the following Nu correlation is derived for a packed bed of shredded tires undergoing pyrolysis and gasification:

$$\mathrm{Nu} = a(X_C) + b(X_C)\mathrm{Re}^{c(X_C)}\mathrm{Pr}^{d(X_C)} \tag{13}$$

with a to d given by Eqs. (9)–(12).

5.2 Validation and Comparison. Several Nu correlations for packed beds of spherical and nonspherical particles are given in the literature [5–8]. Gnielinski's correlation [5] resulted from a combination of Nu correlations around a single sphere for laminar and turbulent flow

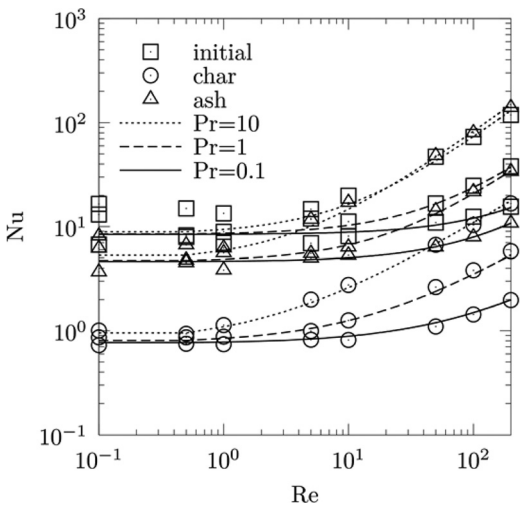

Fig. 4 Re dependent Nu numbers for the packed bed at $X_C = 0$, 0.68, and 1 (initial, char, and ash) and at $\mathrm{Pr} = 0.1$, 1, and 1. The symbols indicate numerically calculated Nu numbers and the solid line the fits given by Eq. (8) and Table 2.

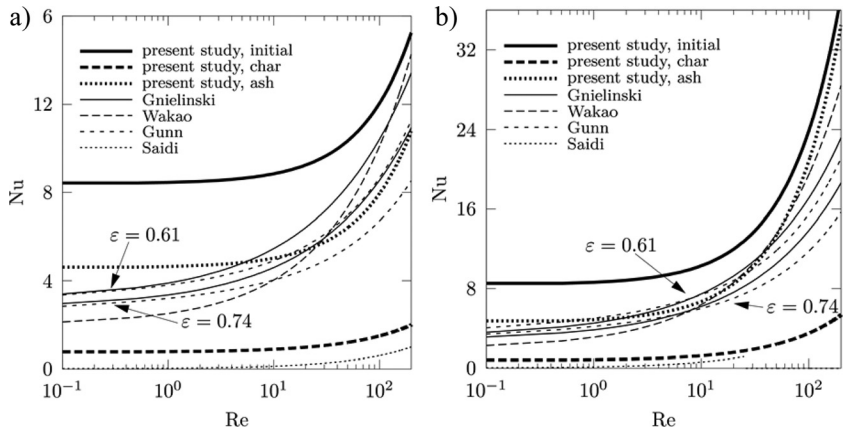

Fig. 5 Nu correlations for packed beds given by Gnielinski ($\varepsilon = 0.61$ and 0.74) [5], Wakao [6], Gunn ($\varepsilon = 0.61$ and 0.74) [7], Saidi [8], and of present study for Pr = 0.1 (*a*) and for Pr = 1 (*b*)

$$\mathrm{Nu_{Gn}} = (1 + 1.5(1-\varepsilon))\mathrm{Nu_s}$$

$$\mathrm{Nu_s} = \mathrm{Nu_{s,min}} + \sqrt{\mathrm{Nu_{s,lam}^2} + \mathrm{Nu_{s,turb}^2}} = \left(2 + \sqrt{\left(0.664\mathrm{Re}^{0.5}\,\mathrm{Pr}^{1/3}\right)^2 + \left(\frac{0.037\mathrm{Re}^{0.8}\,\mathrm{Pr}}{1 + 2.443\mathrm{Re}^{-0.1}\left(\mathrm{Pr}^{2/3} - 1\right)}\right)^2}\right) \tag{14}$$

Wakao's correlation [6] was obtained by fitting experimental results, correcting for axial dispersion if needed

$$\mathrm{Nu_{Wa}} = 2 + 1.1\mathrm{Re}^{0.6}\mathrm{Pr}^{1/3} \tag{15}$$

Gunn's correlation [7] is based on a stochastic model for the packed bed geometry

$$\mathrm{Nu_{Gu}} = \left(7 - 10\varepsilon + 5\varepsilon^2\right)\left(1 + 0.7\mathrm{Re}^{0.2}\mathrm{Pr}^{1/3}\right) + \left(1.33 - 2.4\varepsilon + 1.2\varepsilon^2\right)\mathrm{Re}^{0.7}\mathrm{Pr}^{1/3} \tag{16}$$

Saidi's correlation [8] is derived by fitting experimental results with a packed bed of nonspherical particles with $\varepsilon = 0.8$ to a continuum model

$$\mathrm{Nu_{Sa}} = 0.015 + 0.11\mathrm{Re}^{0.75}\mathrm{Pr}^{0.75} \tag{17}$$

The Nu correlation derived in this study for the reacting packed bed of complex, porous, and nonspherical particles, given by Eq. (13), is compared to those Nu correlations given by the models of Eqs. (14)–(17).

Results of this comparison are shown in Fig. 5 as a function of Re for Pr = 0.1 and 1. For the initial packed bed, the Nu correlations of Eq. (14)–(16) are not appropriate, especially for low Re. Mousa [28] reports measured Nu numbers exceeding 40 for $9 < \mathrm{Re} < 30$ and Pr = 0.7. For the packed bed after pyrolysis (char), consisting of nonspherical and highly porous particles, the Nu numbers lie in the range proposed by Saidi [8] (RMS = 1.2 for $\mathrm{Re}\cdot\mathrm{Pr} < 25$). For the final ash, all the modeled Nu correlations of Eq. (14)–(16) approach the one derived in this study. Ash particles are more spherical-like and less porous. The strong increase in Nu for the packed bed at $X_C = 0$ and 1 at high Re is related to the large Dupuit–Forchheimer coefficient and the larger tortuosities (see Secs. 6 and 7), allowing for superior heat transfer.

Packed beds of random identical overlapping opaque spheres (IOOS, $\varepsilon = \exp(-n\pi d^3/6)$) with corresponding particle sizes and porosities (see Table 1) are generated to investigate the influence of sphere size distribution and sphericity on the effective properties. DPLS is used for the determination of the effective properties. The numerically determined and fitted Nu correlations are depicted in Table 3.

6 Mass—Permeability and Dupuit–Forchheimer Coefficient

6.1 Theory and Results. Flow through porous media is described by Darcy's law [29], which linearly relates the pressure drop to the velocity. For $\mathrm{Re} > 1$, the form drag due to solid obstacles (inertial resistance) gets comparable to the surface drag due to friction (viscous resistance). Thus, an additional term proposed by Forchheimer [30] is introduced. The determination of the permeability, K, and Dupuit–Forchheimer coefficient, F_{DP}, is therefore based on the extended Darcy's law

Table 3 Numerically determined Nu correlations for the three packed beds composed of IOOS with the same porosity and diameter as the reacting packed bed at $X_C = 0$, 0.68, and 1

	Corresponding X_C	Nu	RMS
IOOS ($\varepsilon = 0.61$, $d = 1.14$ mm)	0	$4.608 + 0.360\mathrm{Re}^{0.699}\mathrm{Pr}^{0.538}$	0.04
IOOS ($\varepsilon = 0.74$, $d = 0.97$ mm)	0.68	$3.804 + 0.380\mathrm{Re}^{0.662}\mathrm{Pr}^{0.513}$	0.04
IOOS ($\varepsilon = 0.65$, $d = 0.42$ mm)	1	$2.845 + 0.531\mathrm{Re}^{0.614}\mathrm{Pr}^{0.534}$	0.05

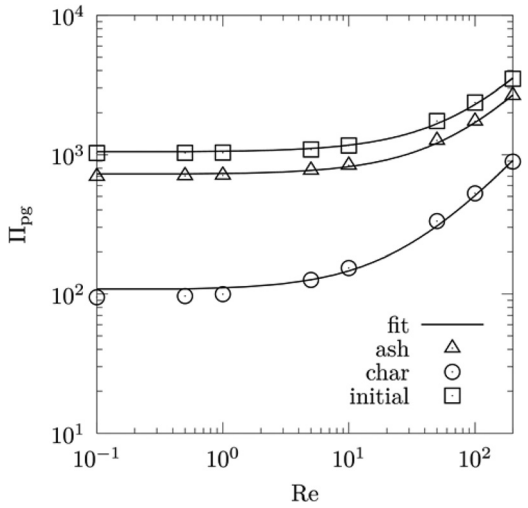

Fig. 6 Dimensionless pressure drop, Π_{pg}, as a function of Re for the three samples of the packed bed at $X_C = 0$, 0.68, and 1 (initial, char, and ash)

$$\nabla p = -\frac{\mu}{K}\bar{\mathbf{u}}_D - F_{DF}\rho\bar{\mathbf{u}}_D|\bar{\mathbf{u}}_D| \tag{18}$$

The nondimensional form for the 1D case yields

$$\Pi_{pg} = c_0 + c_1\mathrm{Re} = -\frac{d^2}{K} - F_{DF}d\mathrm{Re} \tag{19}$$

where $\Pi_{pg} = \nabla p d^2 \mu^{-1} u_D^{-1}$. The coefficients c_0 and c_1 of the linear function are directly related to K and F_{DP}. The pressure variations associated with the artificial abruptly changing flow patterns at the sample's inlet/outlet represent less than 1% of the pressure drop across the sample and therefore are negligible. The dimensionless pressure gradients for the three samples of the packed bed at different X_C are plotted in Fig. 6. The resulting K and F_{DP} are tabulated in Table 4. The highest K of the packed bed is obtained at $X_C = 0.68$ (char). This is consistent with the fact that the highly porous, fractal-like particles evolved during pyrolysis. The lowest F_{DF} is obtained at $X_C = 0.68$. This is again explained by the porous structure of the particles contained in the bed, allowing the fluid to pass through the sample in a less disturbed manner, as verified by the tortuosity distributions calculated in the Sec. 6.4.

The following correlations for K and F_{DF} of a packed bed of shredded tire particles undergoing pyrolysis and gasification are proposed:

$$K(X_C) = -4.03 \cdot 10^{-8}X_C^2 + 3.92 \cdot 10^{-8}X_C + 1.24 \cdot 10^{-9} \tag{20}$$

$$F_{DP}(X_C) = 75'862X_C^2 - 63'255X_C + 10'941 \tag{21}$$

K increased and decreased with X_C while the opposite was observed for F_{DF}. These changes were associated with morphological changes during the reaction. During pyrolysis, the formation of direct flow paths across the packed bed reduced the pressure drop and inertial resistance, leading to higher K and lower F_{DF}. During gasification, the decrease of porosity resulted in higher pressure drop and inertial resistance.

Table 4 X_C dependent permeability and Dupuit–Forchheimer coefficient of the reacting packed bed

	K (m^2)	F_{DF} (m^{-1})	RMS
Initial ($X_C = 0$)	$1.242 \cdot 10^{-9}$	10,941	43.4
Char ($X_C = 0.68$)	$8.817 \cdot 10^{-9}$	4130	14.9
Ash ($X_C = 1$)	$2.444 \cdot 10^{-10}$	23,348	28.6

6.2 Validation and Comparison. K of a medium composed of parallel channels with Hagen–Poiseuille flow is given by [9]

$$K_{cap} = \frac{\varepsilon d^2}{32} \tag{22}$$

The hydraulic radius model [9] based on the Carman–Kozeny theory is given by Eq. (23)

$$K_{hyd} = \frac{\varepsilon^3 d^2}{36k_0\tau(1-\varepsilon)^2} = \frac{\varepsilon^3 d^2}{36k_K(1-\varepsilon)^2} \tag{23}$$

$k_K = k_0\tau$ is the Kozeny constant which is the product of a shape parameter, k_0, and the tortuosity, τ. k_K is approximated to be 5 for packed beds [9]. For fibrous beds, Kyan et al. [31] proposed

$$k_{K,fib} = \frac{\left(62.3\left(\sqrt{\frac{2\pi}{1-\varepsilon}} - 2.5\right)^2(1-\varepsilon) + 107.4\right)\varepsilon^3}{16\varepsilon^6(1-\varepsilon)^4} \tag{24}$$

Kuwabara, Sparrow et al. and Happel et al. [11–13] derived correlations for k_K by solving for the external flow around parallel and perpendicular arranged cylinders and spheres

$$k_{K,par} = \frac{2\varepsilon^3}{(1-\varepsilon)\left(2\ln\left(\frac{1}{1-\varepsilon}\right) - 3 + 4(1-\varepsilon) - (1-\varepsilon)^2\right)} \tag{25}$$

$$k_{K,per} = \frac{\frac{2\varepsilon^3}{1-\varepsilon}}{\frac{1}{1-\varepsilon} - \frac{1-(1-\varepsilon)^2}{1+(1-\varepsilon)^2}} \tag{26}$$

Rumpf et al. [32] showed that for a packed bed of spherical particles with a narrow size distribution, K is well approximated by

$$K_R = \frac{\varepsilon^{5.5}d^2}{5.6} \tag{27}$$

Itoh [33] determined the permeability of a random array of rigid spheres accounting for the so called intermediate layer, a particular state formed around a test sphere. Davis et al. [34] calculated the permeability of a packed bed made of porous particles with an inner permeability, K_{inner}.

For higher Re numbers, MacDonald et al. [15] suggested a formulation to determine F_{DP} based on Ergun's theory

$$F_{DF,MD} = 1.8\frac{1-\varepsilon}{\varepsilon^3 d} \tag{28}$$

Ward [16] proposed

$$F_{DF,W} = \frac{0.55}{\sqrt{K}} \tag{29}$$

Figure 7 compares the DPLS-determined K and F_{DP} of the reacting packed bed at $X_C = 0$, 0.68, and 1 (initial, char, and ash) with those obtained by Eqs. (22)–(29) and models given by Itoh [33] and Davis [34]. For clarity, a packed bed with $K_{inner} = 10^{-10}$ m^2 is assumed for the calculations. ε and d are adapted according to the sample specification for $X_C = 0$, 0.68, and 1 (see Table 1). The values for K and F_{DP} scatter in a range of several orders of magnitude, spanned by the models.

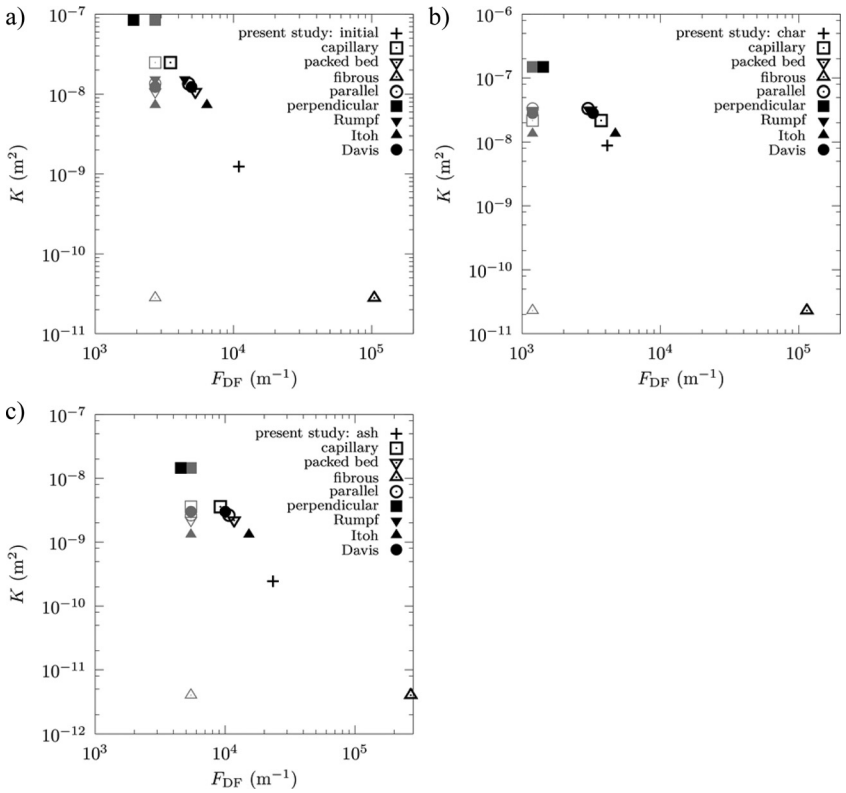

Fig. 7 ***K*** **and** F_{DP} **numerically determined by DPLS with those calculated by models for packed beds with** $K_{inner} = 10^{-10}$ **m^2 and for (*a*):** $\varepsilon = 0.61$, $d = 1.14$ **mm; (*b*):** $\varepsilon = 0.74$, $d = 0.97$ **mm; and (*c*):** $\varepsilon = 0.65$, $d = 0.42$ **mm.** F_{DP} **is calculated by MacDonald (grey, Eq. (28)) and by Ward (black, Eq. (29))**

Permeability and Dupuit–Forchheimer of the corresponding IOOS are depicted in Table 5. The porosity affects significantly K and F_{DP}. This is qualitative in agreement with the results of the complex reacting packed bed.

7 Mass Transfer—Tortuosity and Residence Time

7.1 Theory and Results. Tortuosity, τ, is defined as the ratio of the real length of the connected pore channels to the thickness of the porous sample in the main flow direction

$$\tau = \frac{l_{path}}{l_{sample}} \tag{30}$$

Residence time, t, describes the time required for a fluid particle to flow across the sample. It is defined by

$$t = \int_{l_{path}} \frac{1}{|\mathbf{u}|} \mathrm{d}l \tag{31}$$

Table 5 Permeability and Dupuit–Forchheimer coefficient of the three packed beds composed of IOOS with the same porosity and diameter as the reacting packed bed at $X_C = 0$, **0.68, and 1**

	Corresponding X_C	K (m^2)	F_{DF} (m^{-1})	RMS
IOOS ($\varepsilon = 0.61$, $d = 1.14$ mm)	0	$1.581 \cdot 10^{-8}$	2041	5.23
IOOS ($\varepsilon = 0.74$, $d = 0.97$ mm)	0.68	$3.352 \cdot 10^{-8}$	779	1.88
IOOS ($\varepsilon = 0.65$, $d = 0.42$ mm)	1	$3.451 \cdot 10^{-9}$	3104	4.05

The velocity distribution is used to create sets of 2500 stream lines uniformly distributed over the inlet for each Re number. Their length and the integrated time on the stream line are calculated. Calculated distributions of τ and t for the packed bed at $X_C = 0$, 0.68, and 1 (initial, char, and ash) and $\mathrm{Re} = 1$ are shown in Figs. 8 and 9, respectively. Mean, median, and mode of the calculated distributions of τ and t at $\mathrm{Re} = 1$ are given in Table 6. The following correlations of τ_m and t_m for a packed bed of shredded tire particles undergoing pyrolysis and gasification are derived ($\mathrm{Re} = 1$)

$$\tau_m(X_C) = 0.08X_C^2 - 0.14X_C + 1.26 \tag{32}$$

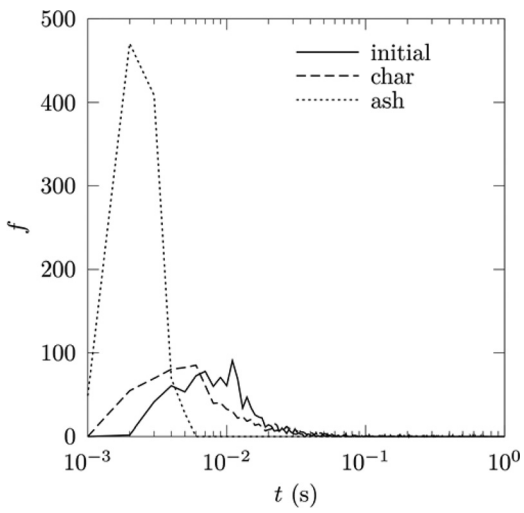

Fig. 8 Residence time distribution at $\mathrm{Re} = 1$ **for the reacting packed bed at** $X_C = 0$, **0.68, and 1 (initial, char, and ash)**

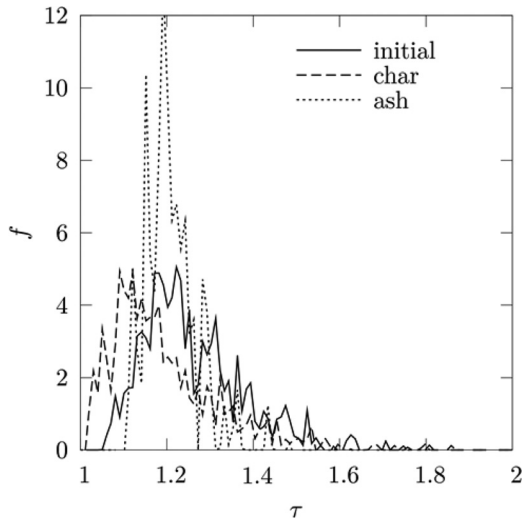

Fig. 9 Tortuosity distribution at Re = 1 for the reacting packed bed at at X_C = 0, 0.68, and 1 (initial, char, and ash)

Table 6 Mean, mode, and median tortuosity and residence time for the packed bed at Re = 1

	τ_m	τ_{mode}	τ_{med}	t_m (s)	t_{mode} (s)	t_{med} (s)
Initial ($X_C = 0$)	1.256	1.184	1.232	0.014	0.011	0.010
Char ($X_C = 0.68$)	1.196	1.094	1.165	0.030	0.006	0.009
Ash ($X_C = 1$)	1.204	1.150	1.197	0.003	0.002	0.003

$$t_m(X_C) = -0.12X_C^2 + 0.10X_C + 0.01 \quad (33)$$

τ at $X_C = 0.68$ is smaller than that at $X_C = 0$ and 1. Since the particles after pyrolysis are highly porous, fluid is able to pass through the packed bed with lower tortuosity. The τ and t distributions at $X_C = 0.68$ exhibits a tail accounting for fluid particles trapped for some time at unconnected pores, resulting in larger residence times.

8 Conclusions

DPLS was applied to a reacting packed bed whose complex 3D geometry was determined by high-resolution CT at different reaction extents. The pyrolysis and gasification of shredded waste tires were chosen as the model reaction due to their significance in solar fuel production processes. The governing conservation equations were solved at the pore-level scale using FV techniques. The convective heat transfer coefficient, permeability, Dupuit–Forchheimer coefficient, tortuosity, and residence time distributions for the reacting packed bed were determined and compared to correlations available in the literature. All effective transport properties were found to be strong functions of the reaction extent. The initial packed bed was characterized by larger Nu numbers than those obtained by the models of Gnielinski or Wakao [5,6] but smaller values than those measured by Mousa [28]. The packed bed after pyrolysis (char) was composed of porous and nonspherical particles. The final packed bed (ash) showed comparable Nu values as those proposed for packed beds of rigid and spherical particles. The packed bed after pyrolysis (char) showed the highest K and the lowest F_{DF}, because of the high inner porosity of particles that enhanced the bed porosity and shortened its tortuosity and residence time. Analytical Nu, K, F_{DF}, τ_m, and t_m correlations for a packed bed undergoing pyrolysis and gasification were derived as a function of the reaction extent. These effective transport properties can in turn be incorporated in volume-averaged (continuum) models for the purpose of design and optimization of packed-bed reactors.

Acknowledgment

This work has been financially supported by the Swiss National Science Foundation under Contract No. 200021-115888 and by the European Commission under Contract No. 212470 (Project HycycleS). We thank C. Suter and the staff of the TOMCAT beamline for the technical support at PSI's SLS and O. Byrde for the technical support with ETH's cluster Brutus. We thank H. Fries for the support with the numerical meshing of complex geometries.

Nomenclature

A_0 = specific surface, m^{-1}
c_0, c_1 = constants in Eq. (19)
c_p = specific heat capacity of fluid, $Jkg^{-1}K^{-1}$
d = particle diameter, m
f = distribution function
F_{DF} = Dupuit–Forchheimer coefficient, m^{-1}
h = heat transfer coefficient, $Wm^{-2}K^{-1}$
k = conductivity of fluid, $Wm^{-1}K^{-1}$
k_k = Kozeny constant
K = permeability, m^2
l = length, m
N_{vox} = number of voxels
n = number density, m^{-3}
Nu = Nusselt number, $Nu = h_{sf}d_{m,ex}k^{-1}$
p = (partial) pressure, Nm^{-2}
Pr = Prandtl number, $Pr = \mu c_p k^{-1}$
Re = Reynolds number, $Re = u_D d_{med,ex}\nu^{-1}$
t = residence time, s
T = temperature, K
u_D = Darcean or superficial velocity, ms^{-1}
X_C = reaction extent (based on C conversion)

Greek

μ = dynamic viscosity of fluid, $kgm^{-1}s^{-1}$
ε = porosity
γ = half bandwidth for REV determination
Π_{pg} = dimensionless pressure gradient, $\Pi_{pg} = \nabla p d^2 \mu^{-1} u_D^{-1}$
ρ = density, $kg\ m^{-3}$
τ = tortuosity
ν = kinematic viscosity of fluid, m^2s^{-1}

Subscripts

cap = capillary
ex = experiment
fib = fibrous
Gn = Gnielinski
Gu = Gunn
hyd = hydraulic
lam = laminar
lm = logarithmic mean
m = mean
min = minimal
med = median
MC = MacDonald
num = numerical
par = parallel
per = perpendicular
R = Rumpf
s = sphere
sf = solid–fluid
Sa = Saidi

tot = total
turb = turbulent
W = Ward
Wa = Wakao

Abbreviations

CT = computed tomography
DPLS = direct pore-level simulation
ETH = Swiss Federal Institute of Technology
FOV = field of view
FV = Finite volume
REV = representative elementary volume
SLS = Swiss Light Source
TOMCAT = tomographic microscopy and coherent radiology

References

[1] von Zedtwitz, P., and Steinfeld, A., 2003, "The Solar Thermal Gasification of Coal—Energy Conversion Efficiency and CO_2 Mitigation Potential," Energy, **28**, pp. 441–456.
[2] Schunk, L., Haeberling, P., Wepf, S., Wuillemin, D., Meier, A., and Steinfeld, A., 2008, "A Receiver-Reactor for the Solar Thermal Dissociation of Zinc Oxide," ASME J. Solar Energy Eng., **130**, p. 0210091.
[3] Piatkowski, N., Wieckert, C., and Steinfeld, A., 2009, "Experimental Investigation of a Packed-Bed Solar Reactor for the Steam-Gasification of Carbonaceous Feedstocks," Fuel Process. Technol., **90**, pp. 360–366.
[4] Whitaker, S., 1999, "The Method of Volume Averaging," *Theory and Applications of Transport in Porous Media*, Vol. 13, J. Bear, ed., Kluwer Academic Publishers.
[5] Gnielinski, V., 1978, Gleichung zu Berechnung der Wärme- und Stoffaustausches in durchströmten ruhenden Kugelschüttungen bei mittleren und grossen Pecletzahlen, Verfahrenstechnik, **12**, pp. 363–366.
[6] Wakao, N., and Kaguei, S., 1982, *Heat and Mass Transfer in Packed Beds*, Gordon and Breach Science Publishers.
[7] Gunn, D., 1978, "Transfer of Heat and Mass to Particles in Fixed and Fluidized Beds," Int. J. Heat Mass Transfer, **21**, pp. 467–476.
[8] Saidi, M., Rasouli, F., and Hajaligol, M., 2006, "Heat Transfer Coefficient for a Packed Bed of Shredded Materials at Low Peclet Numbers," Heat Transfer Eng., **27**, pp. 41–49.
[9] Kaviany, M., 1995, *Principles of Heat Transfer in Porous Media*, Springer-Verlag, New York.
[10] Dullien, F., 1979, *Porous Media Fluid Transport and Pore Structure*, Academic Press, New York.
[11] Kuwabara, S., 1959, "The Forces Experienced by Randomly Distributed Parallel Circular Cylinder or Spheres in a Viscous Flow at Small Reynolds Numbers," J. Phys. Soc. Jpn., **14**, pp. 527–532.
[12] Sparrow, E., and Loeffler, A., 1959, "Longitudinal Laminar Flow Between Cyclinders Arranged in a Regular Array," Am. Inst. Chem. Eng., **5**, pp. 325–330.
[13] Happel, J., and Brenner, H., 1986, *Low Reynolds Number Hydrodynamics*, Martinus Nijhoff Publishers.
[14] Torquato, S., 1990, "Relationship Between Permeability and Diffusion Controlled Trapping Constant of Porous Media," Phys. Rev. Lett., **64**, pp. 2644–2646.
[15] Macdonald, I. F., El-Sayed, M. S., Mow, K., and Dullien, F. A. L., 1979, "Flow Through Porous Media—The Ergun Equation revisited," Ind. Eng. Chem. Fundam., **18**, pp. 199–208.
[16] Ward, J., 1964, "Turbulent Flow in Porous Media," J. Am. Soc. Civ. Eng., **90**, pp. 1–12.
[17] Petrasch, J., Meier, F., Friess, H., and Steinfeld, A., 2008, "Tomography Based Determination of Permeability, Dupuit-Forchheimer Coefficient, and Interfacial Heat Transfer Coefficient in Reticulate Porous Ceramics," Int. J. Heat Fluid Flow, **29**, pp. 315–326.
[18] Haussener, S., Coray, P., Lipiński, W., Wyss, P., and Steinfeld, A., 2010, "Tomography-Based Heat and Mass Transfer Characterization of Reticulate Porous Ceramics for High-Temperature Processing," ASME J. Heat Trans., **132**, p. 023305.
[19] Ferréol, B., and Rothman, D., 1995, "Lattice-Boltzmann Simulation of Flow Through Fontainebleau Sandstone," Transp. Porous Media, **20**, pp. 3–20.
[20] Humby, S., 1999, "Modelling of Flow and Colloids in Porous Media," Ph.D. thesis, University of Surrey, Guildford, UK.
[21] Auzerai, F., Dunsmuir, J., Ferréol, B., Martys, N., Olson, J., Ramakrishnan, T., Rothmann, D., and Schwartz, L., 1996, "Transport in Sandstone: A Study Based on Three Dimensional Microtomography," Geophys. Res. Lett., **23**, pp. 3–20.
[22] Brensdorf, J., Brenner, G., and Dust, F., 2000, "Numerical Analysis of the Pressure Drop in Porous Media Flow With Lattice Boltzmann (BGK) Automata," Comput. Phys. Commun., **129**, pp. 247–255.
[23] Spanne, P., Thovert, J., Jacquin, C., Lindquist, W., Jones, K., and Adler P., 1994, "Synchrotron Computed Microtomography of Porous Media: Topology and Transport," Phys. Rev. Lett., **73**, pp. 2001–2004.
[24] Haussener, S., Lipiński, W., Wyss, P., and Steinfeld, A., 2010, "Tomography-Based Analysis of Radiative Transfer in Reacting Packed Beds Undergoing a Solid-Gas Thermochemical Transformation," ASME J. Heat Trans., **132**, p. 061201.
[25] Streun, A., Böge, A., Dehler, M., Gough, C., Joho, W., Korhonen, T., Lüdeke, A., Marchand, P., Muñoz, Pedrozzi, M., Rivkin, L., Schilcher, T., Schlott, V., Schulz, L., and Wrulich, A., 2001, "Commissioning of the Swiss Light Source," *Proceedings of the 2001 Particle Accelerator Conference*, P. Lucas and S. Webber, eds., IEEE, Piscataway, pp. 224–226.
[26] Stampanoni, M., Groso, A., Isenegger, A., Mikuljian, G., Chen, Q., Bertrand, A., Henein, S., Betemps, R., Frommherz, U., Böhler, P., Meister, D., Lnage, M., and Abela, R., 2006, "Trends in Synchrotron-Based Tomographic Imaging: The SLS Experience," Proc. SPIE, **6318**, pp. M-1–M-14.
[27] Ansys Inc., 2009, Ansys CFX-12.0, www.ansys.com.
[28] Mousa, A., 1984, "Prediction of Gas-Particle Heat Transfer Coefficients by Pulse Technique," Ind. Eng. Chem. Process. Des. Dev., **23**, pp. 805–808.
[29] Darcy, H., 1856, *Les Fontaines Publiques sur le movement des eaux*, Dalmont, Paris.
[30] Forchheimer, P., 1901, "Water Movement Through Ground," Zeitschrift des Vereins Deutscher Ingenieure, **45**, pp. 1782–1788.
[31] Kyan, C., Wasan, D., and Kintner, R., 1970, "Flow of Single-Phase Fluids Through Fibrous Beds," Ind. Eng. Chem. Fundam., **9**, pp. 596–603.
[32] Rumpf, H., and Gupte, A., 1971, "Influence of Porosity and Particle Size Distribution in Resistance Law of Porous Flow," Chem. Eng. Technol., **43**, pp. 367–375.
[33] Itoh, S., 1983, "The Permeability of a Random Array of Identical Rigid-Spheres," J. Phys. Soc. Jpn., **52**, pp. 2379–2388.
[34] Davis, R., and Stone, H., 1993, "Flow Through Beds of Porous Particles," Chem. Eng. Sci., **48**, pp. 3993–4005.